Structures 34 (2021) 1276–1290

Contents lists available at ScienceDirect

Structures

journal homepage: www.elsevier.com/locate/structures

A common framework for the robust design of tuned mass damper techniques to mitigate pedestrian-induced vibrations in lively footbridges

Javier Fernando Jiménez-Alonso [a,*], José Manuel Soria [b], Iván M. Díaz [c], Francisco Guillen-González [d]

[a] Department of Continuum Mechanics and Structural Analysis, Escuela Técnica Superior de Ingeniería, Universidad de Sevilla, Sevilla, Spain
[b] Department of Signal Theory and Communications, Escuela Politécnica Superior, Universidad de Alcalá, Alcalá de Henares, Spain
[c] Department of Continuum Mechanics and Structures, E.T.S. Ingenieros de Caminos, Canales y Puertos, Universidad Politécnica de Madrid, Madrid, Spain
[d] Department of Mathematical Analysis, Universidad de Sevilla, Seville, Spain

ARTICLE INFO

Keywords:
Tuned mass damper
Vibration control
Motion-based design
Reliability multi-objective optimization
Human-induced vibrations
Footbridges
Uncertainty conditions

ABSTRACT

The dynamic response of modern slender footbridges is usually sensitive to both the pedestrian actions and the uncertainties associated with their inherent structural behavior. Thus, tuned mass dampers have been widely integrated in the design of these structures to guarantee the fulfillment of the vibration serviceability limit state during their overall life cycle. Three different techniques of tuned mass dampers (active, semi-active and passive) are usually considered for this purpose. Although there are algorithms for the robust design of each particular technique, however, this specificity makes difficult the implementation of all these techniques in practical engineering applications. Herein, the motion-based design method under uncertainty conditions is proposed and further implemented to create a common framework for the robust design of all these techniques when they are employed to mitigate pedestrian-induced vibrations in slender footbridges. According to this method, the design problem may be transformed into the combination of two sequential sub-problems: (i) a reliability multi-objective optimization sub-problem; and (ii) a decision-making sub-problem. Subsequently, the performance of this proposal has been validated through a numerical case study in which the dynamic response of a steel footbridge has been controlled by three different tuned mass damper techniques designed according to the proposed common framework.

1. Introduction

The dynamic response of modern slender footbridges is sensitive to the pedestrian actions together with the uncertainties associated with their inherent structural behavior [1,2]. Hence, different vibration absorbers have been usually used to control robustly the dynamic response of these civil engineering structures during their overall life cycle [3]. Among these devices, tuned mass dampers (TMD) have been widely employed to mitigate pedestrian-induced vibrations in slender footbridges due to the good balance among their performance, cost and easy installation [4]. A TMD is a mechanical device in which the natural frequency, f_d [Hz], of the vibration absorber is tuned to the natural frequency, f_s [Hz], of the vibration mode of the main structure, which is needed to be controlled. [5]. Thus, the energy dissipated by this control device is maximized when this design requirement is met, and therefore, its performance can be reduced if any modification of the operational and the environmental conditions originates the detuning between the TMD and the structure [5].

In order to guarantee an adequate performance of the tuned mass damper during the overall life cycle of the structure different TMD techniques have been proposed [5]. According to their constitutive laws, these techniques may be classified in three groups [5]: (i) active TMD [6]; (ii) semi-active TMD [7]; and (iii) passive TMD [8]. Despite these different constitutive laws, all these techniques share the same objective, to guarantee the adequate performance of the vibration absorber when the modal properties of the structure change due to the variation of the operational [9] and environmental conditions [10].

To this end, the following mechanisms are employed for each TMD technique: (i) the driving force generated by an actuator in the case of an active TMD (ATMD) [6]; (ii) the variation of its stiffness and/or damping

* Corresponding author at: Department of Continuum Mechanics and Structural Analysis, Escuela Técnica Superior de Ingeniería, Universidad de Sevilla, Camino de los Descubrimientos, s/n, 41092 Sevilla, Spain.
E-mail address: jfjimenez@us.es (J.F. Jiménez-Alonso).

https://doi.org/10.1016/j.istruc.2021.08.070
Received 27 February 2021; Received in revised form 11 August 2021; Accepted 14 August 2021
Available online 28 August 2021

in the case of a semi-active TMD (STMD) [11]; and (iii) the selection of a robust mechanical parameters [12] or the design of an adaptive device [13] for the case of the passive TMD (PTMD). Although ATMD and STMD have shown a higher performance than PTMD when they are used to mitigate vibrations under uncertainty conditions [5] they have a clear limitation when they are employed to control the dynamic behavior of a structure during its overall life cycle, their performance is clearly influenced by the reliability of the external power supply. In order to overcome this problem, a hybrid strategy [14], where a robust performance is assured combining a passive and an intelligent (active or semi-active) behavior, is usually considered. Herein, this hybrid strategy will be considered for the design of the two so-called intelligent control systems (ATMD and STMD).

A great effort has been made by the scientific community during the last fifty years to assist structural engineers in the design of these different TMD techniques, proposing and formulating multiple algorithms and control laws under deterministic [15] and stochastic conditions [16]. Among these algorithms, special attention has been paid to the optimum design of these vibration absorbers [17]. Two are normally the objectives of these design algorithms [18]: (i) the optimum placement of the vibration absorber; and (ii) the optimum sizing of the vibration absorber. Assuming that the vibration absorber is located at its optimum position, two type of methods are usually employed to maximize its performance [18]: (i) analytical [19] and; (ii) numerical methods [20].

These numerical methods, based on the theory of structural optimization [21], are currently employed for the design of TMDs to mitigate vibrations in civil engineering applications [22]. According to these optimization methods, the design problem may be formulated either as a constrained single-objective optimization problem or a multi-objective optimization problem.

In spite of the high efficiency of these algorithms, all they share a common drawback, they have been usually developed for a particular vibrations absorber, being difficult to establish a common framework which simplifies the practical implementation of these damping devices in real-world engineering applications.

In order to shed light on this issue, the motion-based design method [5] under uncertainty conditions is presented and further implemented herein to establish a common framework which assists structural engineers in the design of different TMD techniques for practical engineering applications. The motion-based design method is a particular case within the more general performance-based design method [21] in which the design requirements are defined in terms of the fulfilment of the vibration serviceability limit state of the structure.

In particular, a common framework has been approached herein for the design of three different types of vibrations absorbers when these control systems are used to reduce the pedestrian-induced vibrations in slender footbridges under uncertainty conditions. As assumption, a hybrid strategy has been considered herein for the design of these damping devices. This design method had been previously proposed and implemented by the authors for the robust design of passive TMD [12]; and herein the method is generalized to be also employed for the design of intelligent (active and semi-active) TMDs [23]. Thus, the main contribution of this study is the proposal of a common framework for the structural design of slender footbridges integrated with different TMD techniques under uncertainty conditions.

According to the motion-based design method [5], the design problem may be formulated combining two sequential sub-problems: (i) a multi-objective optimization sub-problem; and (ii) a decision-making sub-problem. As result of the multi-objective optimization sub-problem, a set of non-dominated solutions, the so-called Pareto front, is obtained. As result of the decision-making sub-problem, the best solution among the different elements of the Pareto front is determined.

When this design method is implemented to solve the sizing problem for the different TMD techniques, this problem may be formulated considering the following aspects:

(i) the design variables are the mechanical parameters and the driving forces (in the case of the active or semi-active TMD) which governs the structural behavior of the vibration absorber;
(ii) the different elements of the multi-objective function are defined in terms of the cost of the vibration absorber and the design requirements of the designer [24];
(iii) a search domain for each design variable is considered to guarantee the physical meaning of the solution obtained;
(iv) a nature-inspired computational algorithm is considered to solve the optimization sub-problem [25] due to the non-linear relation between the design variables and the objective function; and
(v) an additional condition is included to solve the decision-making sub-problem.

As the main objective for the design of the different TMD techniques is to mitigate the vibrations of the main structure, the design requirements can usually be defined in terms of the fulfilment of the vibration serviceability limit state (VSLS) of the structure.

Additionally, this design method may be easily adapted to take into account the uncertainties associated with both the variability of the pedestrian actions [26] and the modification of the modal properties of the structure originated by the shift of the operational [9] and environmental conditions [27]. The main effect of these uncertainty sources in the behavior of the TMD is the detuning between the structure and the vibration absorber with the subsequent performance decline [28]. In order to overcome this problem, two different alternatives are usually adopted [23]: (i) the modification of some of the mechanical parameters, which govern the behavior of the vibration absorber, to achieve an adequate adaptation of the device to the new design conditions [29]; and (ii) to design the vibration absorber with such as robust mechanical parameters that an adequate behavior of the structure is assured even if a stochastic behavior of the design conditions is expected [16].

For the particular case of footbridges subjected to pedestrian action, the second alternative can be implemented easily, since the uncertainty associated with the mentioned phenomena occurs in a different temporal-scale, so both phenomena can been simulated independently [16]. Therefore, on the one hand, the uncertainty associated with the pedestrian load has been considered herein following the recommendations of Synpex guidelines [4]; and, on the other hand, the mentioned structural uncertainties have been simulated via the re-formulation of the second term of the multi-objective function and the additional condition of the decision-making sub-problem [30]. In this manner, the fulfilment of the VSLS must be re-defined according to a stochastic approach.

For this purpose, two methods may be considered: (i) a probabilistic method [31]; and (ii) a fuzzy set method [32]. Due to engineering practitioners are more used to probability theory than fuzzy set theory, a probabilistic method, a reliability analysis [33], has been considered herein. Hence the probability of fulfilment of the VSLS has been computed via a reliability index, $\beta(\{\theta\})$. Monte Carlo simulations have been used to determine numerically this reliability index [31]. Accordingly, the re-formulation of the motion-based design problem considering these uncertainty conditions, allows determining a robust design for the different TMD techniques [34].

Finally, the performance of this proposal has been assessed via a comparative case-study in which different TMD techniques have been designed to mitigate the pedestrian-induced vibrations in a slender steel footbridge [35].

The paper is organized as follows. In section 2, a TMD–footbridge interaction model is formulated and further implemented for the numerical assessment of the dynamic response of controlled footbridges under pedestrian action. Subsequently, in section 3, the motion-based design method under uncertainty conditions is presented and further adapted for the TMD design. Later, in section 4, a numerical case-study, based on a slender steel footbridge, is illustrated herein. The performance of three different TMD techniques (active, semi-active and

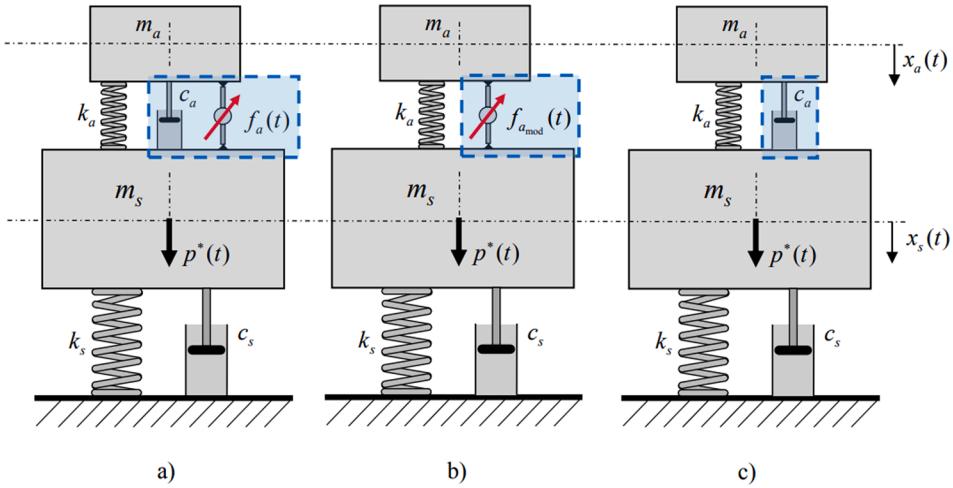

Fig. 1. Different TMD techniques in term of their constitutive behavior: a) active (ATMD): b) semi-active (STMD) and c) passive (PTMD).

passive), designed according to the proposed motion-based design method, is analyzed herein. Finally, some concluding remarks are included in section 5 to finish the paper.

2. Tuned mass Damper-Footbridge interaction model under pedestrian load

A TMD may be decomposed in four elements [23] considering its most general configuration (ATMD): (i) a sprung mass, m_a [kg]; (ii) a viscous damper (dashpot), characterized by its damping coefficient, c_a [sN/m]; (iii) a spring, characterized by its stiffness coefficient, k_a [N/m]; and (iv) an actuator characterized by its equivalent driving force, $f_a(t)$ [N]. In order to illustrate the configuration of the different TMD techniques Fig. 1 shows the main mechanical parameters considered to simulate the dynamic behaviour of each TMD together with the main structure. Herein it is assumed that the behaviour of the structure may be approximated by an equivalent single degree of freedom system (modal coordinates) in which: (i) m_s is the effective mass [kg];c_s is the effective damping [sN/m]; and k_s is the effective stiffness [N/m] of the considered vibration mode.

As it is shown in Fig. 1, the control force generated by each TMD may be decomposed in different terms. Thus, for the ATMD, the control force is generated by the spring, the damper and the actuator; for the STMD, the control force is generated by the spring and the actuator; and for the PTMD, the control force is generated by the spring and the damper. Although different mechanisms have been proposed [36,37] for the design of a STMD (via the modification of its stiffness or damping), herein the semi-active behaviour has been simulated via a virtual actuator, $f_{a_{mod}}(t)$, which models the force generated by a variable damping dashpot (for instance a magnetorheological damper [38]).

For practical engineering applications, the so-called H_∞ design criterion [19] has been widely employed [30]. According to this design criterion, the frequency ratio, $\delta_a = f_d/f_s$, and the damping ratio, ζ_a, of the TMD may be determined in terms of its mass ration,$\mu = m_a/m_s$,

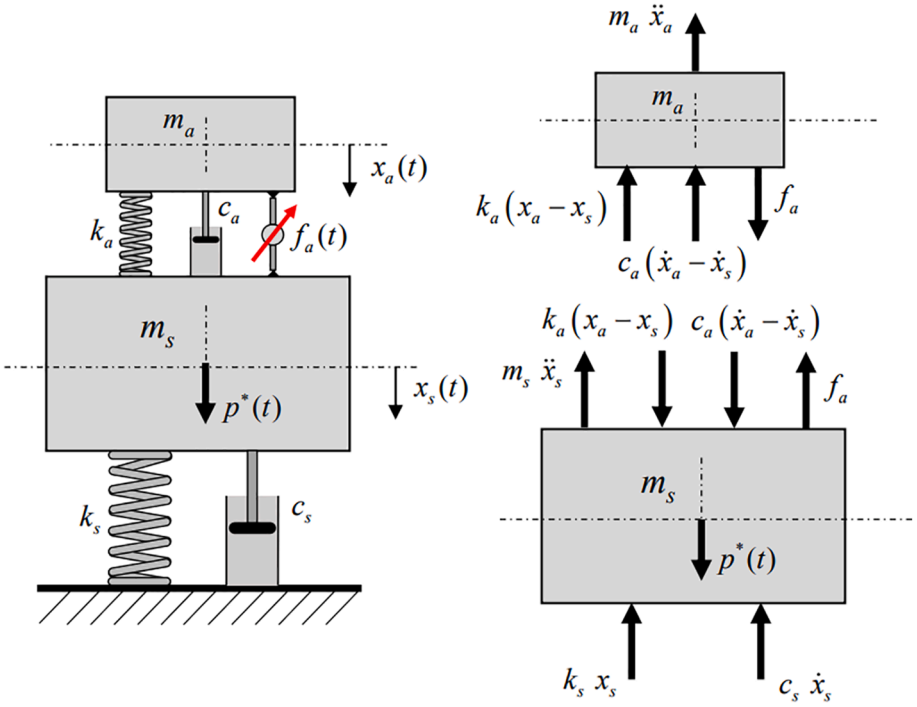

Fig. 2. TMD-footbridge interaction model.

(being m_a the TMD mass and m_s the effective mass of the considered vibration mode) as follows [39]:

$$\delta_a = \frac{1}{1+\mu} \tag{1}$$

$$\zeta_a = \sqrt{\frac{3\mu}{8(1+\mu)}} \tag{2}$$

This design criterion is assumed herein for the tuning of the TMD. On the other hand, these ratios are related to the mechanical parameters of the TMD via the following relationships [4]:

$$c_a = 4 \cdot m_a \cdot \pi \cdot \delta_a \cdot f_s \cdot \zeta_a \tag{3}$$

$$k_a = m_a \cdot (2 \cdot \pi \cdot \delta_a \cdot f_s)^2 \tag{4}$$

In order to compute numerically the response of the structure equipped with the mentioned vibrations absorber, a TMD-footbridge interaction model must be formulated. Herein, the implementation of this interaction model has been divided in four steps: (i) the development of a mathematical model; (ii) the definition of the pedestrian load; (iii) the definition of the driving force; and (iv) the numerical integration of the resulting equations of motion.

For this purpose, the following hypothesis have been assumed herein:

(i) the behavior of the footbridge is simulated via a single vibration mode (modal coordinates), hence it is assumed that only a vibration mode is prone to vibrate;
(ii) the TMD is modelled via a single degree of freedom system (physical coordinates);
(iii) the TMD is modelled in a general way (ATMD), thus the interaction model allows simulating any TMD technique just removing the required element of the equation of motion;
(iv) the pedestrian load is simulated by an equivalent harmonic load according to the recommendations of Synpex guidelines [4]; and
(v) the TMD is located at the antinode of the considered vibration mode.

Fig. 2 shows a scheme of the proposed interaction model. The equations of motion are obtained via the application of the second Newton's law to the two masses (damping device and equivalent modal mass) and assuming that the effect of gravity on the dynamic response of the interaction model under pedestrian load may be despised. The resultant equations may be expressed as follows:

$$m_s \ddot{x}_s(t) + c_s \dot{x}_s(t) + k_s x_s(t) + k_a(x_s(t) - x_a(t)) + c_a(\dot{x}_s(t) - \dot{x}_a(t)) = p^*(t) - f_a(t) \tag{5}$$

$$m_a \ddot{x}_a(t) + c_a(\dot{x}_a(t) - \dot{x}_s(t)) + k_a(x_a(t) - x_s(t)) = f_a(t) \tag{6}$$

where $p^*(t) = \phi^T p(t)$ [N] is the projection of the pedestrian load on the considered vibration mode (being $p(t)$ the pedestrian load [N], ϕ the considered vibration mode and ^{T} the transpose function); $\ddot{x}_s(t)$ [m/s^2], $\dot{x}_s(t)$ [m/s] and $x_s(t)$ [m] are respectively the acceleration, velocity and displacement of the structure; $\ddot{x}_a(t)$ [m/s^2], $\dot{x}_a(t)$ [m/s] and $x_a(t)$ [m] are respectively the acceleration, velocity and displacement of the TMD; and $f_a(t)$ [N] is the driving force generated by the actuator of the ATMD.

Eqns. (5) and (6) can be re-organized in matrix form as follows:

$$\begin{bmatrix} m_s & 0 \\ 0 & m_a \end{bmatrix} \begin{Bmatrix} \ddot{x}_s(t) \\ \ddot{x}_a(t) \end{Bmatrix} + \begin{bmatrix} c_s + c_a & -c_a \\ -c_a & c_a \end{bmatrix} \begin{Bmatrix} \dot{x}_s(t) \\ \dot{x}_a(t) \end{Bmatrix} + \begin{bmatrix} k_s + k_a & -k_a \\ -k_a & k_a \end{bmatrix} \begin{Bmatrix} x_s(t) \\ x_a(t) \end{Bmatrix} = \begin{Bmatrix} 1 \\ 0 \end{Bmatrix} p^*(t) + \begin{Bmatrix} -1 \\ 1 \end{Bmatrix} f_a(t) \tag{7}$$

Table 1
Traffic classes and pedestrian densities according to Synpex guidelines.

Traffic Class	Density$d$	Description
TC1	15 P	Very weak traffic
TC2	<0.20 P/m^2	Comfortable and free walking
TC3	<0.50 P/m^2	Unrestricted walking, significantly dense traffic
TC4	<1.00 P/m^2	Uncomfortable situation, obstructed walking
TC5	<1.50 P/m^2	Unpleasant walking, very dense traffic

$$[M]\{\ddot{x}(t)\} + [C]\{\dot{x}(t)\} + [K]\{x(t)\} = \{B_0\}p^*(t) + \{B_c\}f_a(t) \tag{8}$$

where $[M] = \begin{bmatrix} m_s & 0 \\ 0 & m_a \end{bmatrix}$ is the mass matrix; $[C] = \begin{bmatrix} c_s+c_a & -c_a \\ -c_a & c_a \end{bmatrix}$ is the damping matrix; $[K] = \begin{bmatrix} k_s + k_a & -k_a \\ -k_a & k_a \end{bmatrix}$ is the stiffness matrix; $\{B_0\}$ is the input vector associated with the pedestrian load; $\{B_c\}$ is the input vector associated with the driving force; $\{\ddot{x}(t)\}$ is the acceleration vector; $\{\dot{x}(t)\}$ is the velocity vector and $\{x(t)\}$ is the displacement vector.

Subsequently, Eqn. (8) is transformed into a state-space formulation [23] as follows:

$$\{\dot{z}(t)\} = [A]\{z(t)\} + [B]\{u(t)\} \tag{9}$$

$$\{y(t)\} = [E]\{z(t)\} + [D]\{u(t)\} \tag{10}$$

$$[A] = \begin{bmatrix} 0 & I \\ -[M]^{-1}[K] & -[M]^{-1}[C] \end{bmatrix} \tag{11}$$

$$[B] = \begin{bmatrix} 0 \\ -[M]^{-1}[B_0] \end{bmatrix} \tag{12}$$

$$[E] = -[E_a][[M]^{-1}[K] \quad [M]^{-1}[C]] \tag{13}$$

$$[D] = [E_a][M]^{-1}[B_0] \tag{14}$$

where $\{z(t)\} = \begin{Bmatrix} x_s(t) & x_a(t) & \dot{x}_s(t) & \dot{x}_a(t) \end{Bmatrix}$ is the state vector (defined in terms of the displacement and velocities of both the footbridge and the TMD); $\{u(t)\}$ is the input vector; $\{y(t)\}$ is the output vector (defined as the acceleration experienced by the footbridge); $[A]$ is the state matrix; $[B]$ is the input matrix; $[E]$ is the output matrix; $[D]$ is the feedthrough matrix; and $[E_a]$ is the acceleration matrix (which indicates the elements where the acceleration is computed).

Subsequently, the definition of the pedestrian load, $p(t)$, is taken from the recommendations of Synpex guidelines [4]. According to this guidelines, the walking pedestrian load, $p(t)$, may be simulated via an equivalent harmonic force:

$$p(t) = 280 \cdot \cos(2\pi \cdot f_p \cdot t) \cdot n_{eq} \cdot \psi(f_p) \text{ [N]} \tag{15}$$

where 280 [N] is the vertical dynamic load factor of a single walking pedestrian force; f_p [Hz] is the step frequency (it is assumed that it equals the natural frequency of the footbridge, f_s); n_{eq} is the equivalent number of pedestrians on the footbridge [P = Pedestrian] (number of synchronized pedestrians that originate the same dynamic structural response as n_p arbitrary pedestrians with a randomly distributed step frequency); and $\psi(f_p)$ is the reduction coefficient [-], which takes into account the probability that the footfall frequency approaches the natural frequency under consideration.

The equivalent number of pedestrians, n_{eq}, may be determined from the following expression:

$$n_{eq} = \begin{matrix} 10.8\sqrt{\zeta_s \cdot n_p} \\ 1.85\sqrt{n_p} \end{matrix} \text{ if } \begin{matrix} d < 1 \text{ P/m}^2 \\ d \geq 1 \text{ P/m}^2 \end{matrix} \tag{16}$$

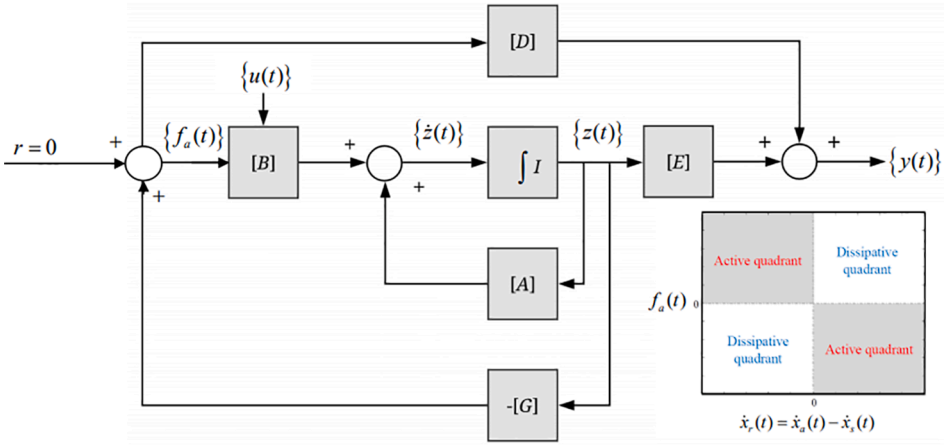

Fig. 3. Flowchart for the design of a feedback controller in a state-space formulation.

where d is the pedestrian density [P/m^2]; ζ_s is the structural damping ratio [-]; and n_p is the number of pedestrians on the footbridge [P]. The pedestrian density, d, is usually set by the designer depending on the expected pedestrian traffic on the footbridge. Table 1 shows the relation between the pedestrian traffic and the pedestrian density according to the recommendations of Synpex guidelines [4].

Finally, the aforementioned reduction coefficient, $\psi(f_p)$, may be obtained from:

$$\psi(f_p) = \begin{cases} 0 & f_p < 1.25 \\ \frac{1}{0.45}(f_p - 1.25) & 1.25 \le f_p < 1.7 \\ 1 & 1.7 \le f_p < 2.1 \\ 1 - \frac{1}{0.2}(f_p - 2.1) & 2.1 \le f_p < 2.3 \\ 0 & 2.3 \le f_p < 2.5 \\ \frac{0.25}{0.9}(f_p - 2.5) & 2.5 \le f_p < 3.4 \\ 0.25 & 3.4 \le f_p < 4.2 \\ 0.25 - \frac{0.25}{0.4}(f_p - 4.2) & 4.2 \le f_p < 4.6 \\ 0 & 4.6 \le f_p \end{cases} \text{ if } [\text{Hz}] \tag{17}$$

The driving force, $f_a(t)$, is determined via the implementation of a feedback controller to the abovementioned system under its state space formulation [40]. Fig. 3 shows the general layout of the considered feedback controller where the driving force, $f_a(t)$, may be determined in terms of a gain matrix, $[G]$, and the state vector, $\{z(t)\}$. The implementation of this feedback controller allows modifying the system equation as follows:

$$\{\dot{z}(t)\} = [A]\{z(t)\} + [B_0]\{p(t)\} - [B_c]\{f_a(t)\} \tag{18}$$

$$\{\dot{z}(t)\} = [A]\{z(t)\} + [B_0]\{p(t)\} - [B_c][G]\{z(t)\} \tag{19}$$

$$\{\dot{z}(t)\} = ([A] - [B_c][G])\{z(t)\} + [B_0]\{p(t)\} \tag{20}$$

where $[B_0]$ and $[B_c]$ are obtained from Eqn. (12) considering as pattern load vectors $\{B_0\}$ and $\{B_c\}$ respectively.

There are several algorithms [23] to determine, $[G]$. Among these algorithms, the linear quadratic regular (LQR) method [23] has been considered herein due to its extensive use for practical engineering applications. According to this method, the value of the matrix gain, $[G]$, is obtained via the minimization of the following performance-index function, J:

$$J = \int_0^{t_f} \left[\{z(t)\}^T[Q]\{z(t)\} + \{[G]\{z(t)\}\}^T[R]\{[G]\{z(t)\}\}\right] dt \tag{21}$$

where $[Q]$ and $[R]$ are two positive-defined weighting matrices; and t_f [sec] is the integration time. These matrices may be selected in terms of the mass, $[M]$, and stiffness, $[K]$, matrices of the interaction model as follows [41]:

$$[Q] = \alpha_d \begin{bmatrix} [K] & 0 \\ 0 & [M] \end{bmatrix} \text{and} [R] = \beta_d [I] \tag{22}$$

where α_d [–] and β_d [–] are the weighting factors.

Additionally, in order to adapt the value of the driving force, $f_a(t)$, determined by the LQR controller, to the particular case of a STMD (for instance to mimic the effect of a magneto-rheological damper) the following relationship has been considered (clipped force method [42]):

$$f_{a_{mod}}(t) = \begin{cases} sgn(f_a(t))\cdot f_{max} & f_a(t)\cdot\dot{x}_r(t) < 0 \text{ and } |f_a(t)| > f_{max} \\ f_a & \text{when } f_a(t)\cdot\dot{x}_r(t) < 0 \text{ and } f_{min} < |f_a(t)| < f_{max} \\ sgn(f_a(t))\cdot f_{min} & f_a(t)\cdot\dot{x}_r(t) > 0 \text{ or } |f_a(t)| < f_{min} \end{cases} \tag{23}$$

where $\dot{x}_r(t)$ [m/s] is the relative velocity, $\dot{x}_r(t) = \dot{x}_a(t) - \dot{x}_s(t)$; $sgn()$ is the sign function; and f_{min} [N] and f_{max} [N] are, respectively, the minimum and maximum dissipative force. Thus, Fig. 3 shows the operating areas of the driving force in terms of both the relative velocity, $\dot{x}_r(t)$, and the TMD technique.

Finally, the response of the TMD-footbridge interaction model can be computed via the integration of the above state space system using a Runge-Kutta method as it is implemented in the Matlab suite of software [43].

3. Motion-based design under uncertainty conditions

Based on the previous TMD-footbridge interaction model, the dynamic response of the controlled footbridge may be obtained as follows:

(i) to develop a linear model of the TMD-footbridge interaction model in the state space domain;
(ii) to tune the TMD for a particular value of the mass ratio, μ, according to some design criterion (herein the H_∞ design criterion has been considered);
(iii) to establish a value for the weighting factors, α_d and β_d;

Table 2
Comfort classes in terms of the allowable acceleration ranges.

Comfort Level	Comfort Degree	Allowable acceleration $\ddot{x}_{lim}$ [m/s^2]
CL 1	Maximum	<0.5
CL 2	Medium	0.5–1.0
CL 3	Minimum	1.0–2.5
CL 4	Unacceptable	>2.5

(iv) to determine the optimum value of the driving force, $f_a(t)$ or $f_{a_{mod}}(t)$; and
(v) to simulate numerically the response of the linear system.

Hence, this process may be repeated iteratively (modifying the triples, $\{\mu \quad \alpha_d \quad \beta_d\}$) until the maximum acceleration of the structures, $\ddot{x}_{s,max}$, was lower than an allowable value, $\ddot{x}_{lim}$ (the fulfilment of the VSLS according to Synpex guidelines [4]). According to this, the design problem may be formulated as a sizing structural problem [21]. The objective of this problem is to find the value of some mechanical parameters of the control system which minimize its cost without compromising the fulfilment of some design requirements established by the designer.

There are two alternatives to define this sizing problem depending on the way in which the design requirements are considered [30]. On the one hand, if the design requirements are considered as constraints, the design problem may be formulated as a constrained optimization problem. On the other hand, if the design requirements are considered in the terms of the objective function, the design problem may be formulated as a multi-objective optimization problem. As result of the first approach, a single solution is obtained, while as result of the second approach, a set of non-dominated solutions is obtained, the so-called Pareto front. Thus, a subsequent decision-making problem must be solved, the selection of the best solution among the different elements of the Pareto front. An additional condition must be included for this purpose. Thus, the general formulation of a multi-objective optimization problem may be expressed as follows [13]:

$$\begin{gathered}\text{Find } \{\theta\} = \{\theta_1 \quad \cdots \quad \theta_i \quad \cdots \quad \theta_{n_d}\} \\ \text{Minimizing} \{f(\{\theta\})\} = \{f_1(\{\theta\}) \quad \cdots \quad f_j(\{\theta\}) \quad \cdots \quad f_{n_s}(\{\theta\})\} \\ \text{Subjected to } \{\theta^l\} \le \{\theta\} \le \{\theta^u\}\end{gathered} \tag{24}$$

where $\{\theta\}$ is the vector of design variables; θ_i is the i^{th} term of the vector of design variables; n_d is the number of design variables; $\{f(\{\theta\})\}$ is the vector which defines the multi-objective function; $f_j(\{\theta\})$ is the j^{th} term of the multi-objective function; n_s is the number of terms of multi-objective function;$\{\theta^l\}$ is the vector of the lower bound of the design variables; and $\{\theta^u\}$ is the vector of the upper bound of the design variables.

Herein, the motion-based design method is formulated based on the mentioned multi-objective approach. Thus, the design problem may be transformed into the combination of two sequential sub-problems [30]: (i) a multi-objective optimization problem; and (ii) a decision-making problem. The objective of this design problem is to find the value of the constitutive parameters of the TMD, that minimizing its cost, grantees the fulfilment of the VSLS of the structure. A hybrid strategy has been considered for the design of the ATMD and STMD techniques. Thus, the motion-based design method is a sizing structural optimization method whose design requirements are defined in terms of the allowable motion of the structure (fulfilment of the VSLS).

The general formulation is now applied to our design problem, thus the multi-objective function, $\{f(\{\theta\})\}$, is proposed to be:

$$\{f(\{\theta\})\} = \{f_1(\{\theta\}) \quad f_2(\{\theta\})\} = \left\{ \mu \quad \frac{\ddot{x}_{s,max}(\{\theta\})}{\ddot{x}_{lim}} \right\} \tag{25}$$

where the first term of the objective function, $f_1(\{\theta\})$, reflects the cost of the vibration absorbers and the second term, $f_2(\{\theta\})$, reflects the level of fulfilment of the VSLS of the footbridge. As Table 2 shows, the recommendations of Synpex guidelines [4] has been considered herein to establish the allowable acceleration, $\ddot{x}_{lim}$.

Additionally, as design variables, $\{\theta\}$, some of the mechanical parameters of the TMD are usually considered (depending on the TMD technique adopted as it is illustrated in Fig. 1). The search domain of these design variables is usually determined by the previous experience and engineering judgement of the designer. Finally, as the relation between the design variables and the objective function is nonlinear, nature-inspired computational algorithms are usually employed to solve the problem [12]. Herein, genetic algorithms have been considered due to their high efficiency to solve complex non-linear optimization problems [25].

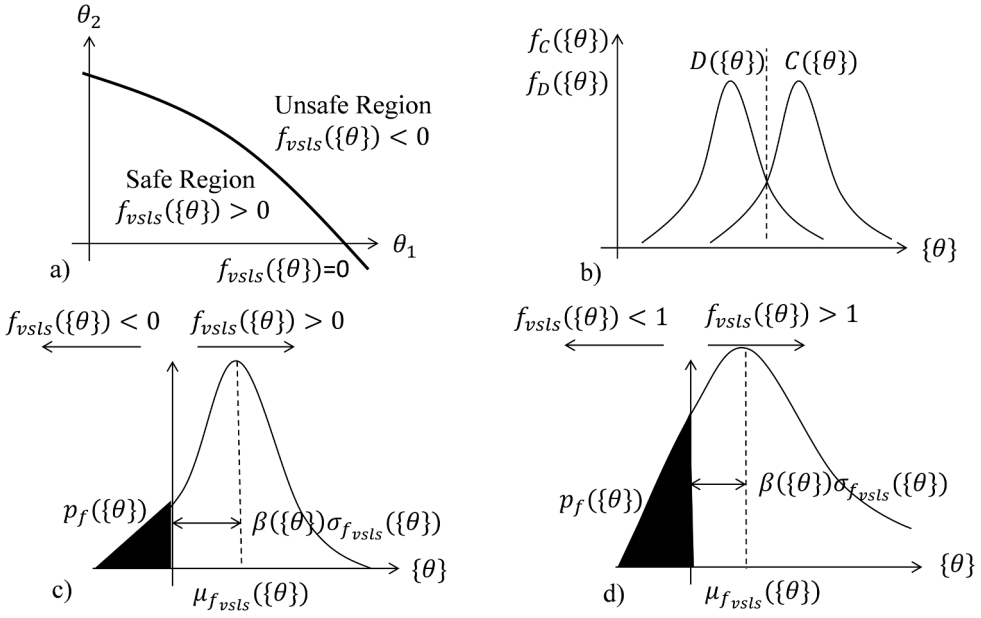

Fig. 4. Reliability analysis: a) Regions of interest; b) Definition of the probability of failure, $p_f(\{\theta\})$; c) $f_{vsls}(\{\theta\})$ following a normal probability density function; and d) $f_{vsls}(\{\theta\})$ following a log-normal probability density function.

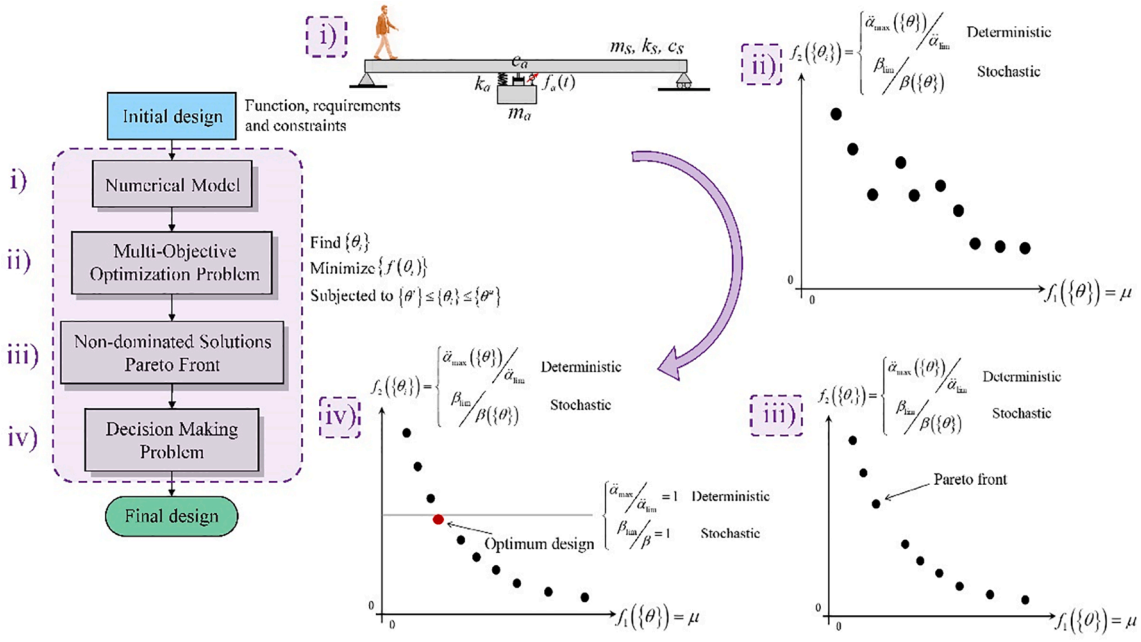

Fig. 5. Flowchart of the motion-based design method for the design of tuned mass dampers.

As result of this optimization problem, a Pareto front is obtained. In order to solve the decision-making problem consisting in the selection of the best solution among the different elements of the Pareto front, an additional condition has been included, $\frac{\ddot{x}_{s,max}(\{\theta\})}{\ddot{x}_{lim}} = 1$. The intersection point between the Pareto front and the line, which represents the additional condition, establishes the solution to this deterministic design problem.

Subsequently, the problem defined by Eqs. (24) and (25) must be re-formulated to take into account for the abovementioned uncertainties. To this end, two approaches may be adopted for the motion-based design method: either a probabilistic approach [30] or a fuzzy logic approach [32].

Herein a probabilistic approach, a reliability analysis [33], has been considered for this purpose. According to this method, the VSLS may be re-formulated according to the following limit state function [33]:

$$f_{vsls}(\{\theta\}) = C(\{\theta\}) - D(\{\theta\}) \tag{26}$$

where $C(\{\theta\})$, the capacity of the structure, and $D(\{\theta\})$, the demand by the external actions, are assumed as random variables. Fig. 4a shows a representation of function, $f_{vsls}(\{\theta\})$. The search domain of the design variables is divided into two regions: safe and unsafe. In this manner, there are many possible sets of solutions which lie into the safe domain. Thus, an additional criterion must be included in order to select the optimum solution among all the safe solutions. The solution with the least probability of failure has been regarded as the optimum solution.

Fig. 4b illustrates the probability density functions of the capacity, $C(\{\theta\})$, and the demand, $D(\{\theta\})$, of the structure for the VSLS. The common area under these two functions defines the probability of failure, $p_f(\{\theta\})$ [38]. Thus, the probability of failure, $p_f(\{\theta\})$, depends on the definition of the limit state function, $f_{vsls}(\{\theta\})$, and its probability distribution function.

Fig. 4 also illustrates the probability distribution function of the limit state function, $f_{vsls}(\{\theta\})$, assuming two possible behaviours: (i) normal distribution (Fig. 4c); and (ii) log-normal distribution (Fig. 4d). For each particular case, it must be checked which is the probability distribution function that better characterizes the limit state function [33].

When the limit state function, $f_{vsls}(\{\theta\})$, follows a normal probability distribution function, the probability of failure, $p_f(\{\theta\})$, may be computed via the following expression [44] (Fig. 4c):

$$p_f(\{\theta\}) = P[C(\{\theta\}) - D(\{\theta\}) < 0] = P[f_{vsls}(\{\theta\}) < 0] = F_{f_{vsls}}(0) = \Phi\left(-\frac{\mu_{f_{vsls}}(\{\theta\})}{\sigma_{f_{vsls}}(\{\theta\})}\right) = \Phi(-\beta(\{\theta\})) \tag{27}$$

where $F_{f_{vsls}}(0)$ is the cumulated probability distribution function of $f_{vsls}(\{\theta\})$; $\mu_{f_{vsls}}(\{\theta\})$ is the mean of the probability distribution function of $f_{vsls}(\{\theta\})$; $\sigma_{f_{vsls}}(\{\theta\})$ is the standard deviation of the probability distribution function of $f_{vsls}(\{\theta\})$; $\Phi()$ stands for the standard normal probability distribution function; and $\beta(\{\theta\})$ is the reliability index [44].

Meanwhile, when the VSLS function, $f_{vsls}(\{\theta\})$, follows a log-normal probability distribution function, the limit state is usually defined by Eq. (28), and the probability of failure, $p_f(\{\theta\})$, may be computed as Eq. (29) [44] (Fig. 4d):

$$f_{vsls}(\{\theta\}) = \frac{C(\{\theta\})}{D(\{\theta\})} \tag{28}$$

$$p_f(\{\theta\}) = P\left[\frac{C(\{\theta\})}{D(\{\theta\})} < 1\right] = \Phi\left(\frac{ln(\mu_C(\{\theta\})/\mu_D(\{\theta\}))}{(\sigma^2_{lnC}(\{\theta\}) + \sigma^2_{lnD}(\{\theta\}))^{1/2}}\right) = \Phi(\beta(\{\theta\})) \tag{29}$$

where $ln()$ is the natural logarithm function; $\mu_C(\{\theta\})$ is the mean of the probability distribution function of the capacity of the structure, $C(\{\theta\})$; $\mu_D(\{\theta\})$ is the mean of the probability distribution function of the demand of the structure, $D(\{\theta\})$; $\sigma_{lnC}(\{\theta\})$ is the standard deviation of the natural logarithm of the probability distribution function of the capacity of the structure, $C(\{\theta\})$; and $\sigma_{lnD}(\{\theta\})$ is the standard deviation of the natural logarithm of the probability distribution function of the demand of the structure, $D(\{\theta\})$.

Therefore, the VSLS is met if the reliability index, $\beta(\{\theta\})$, is greater than an allowable reliability index, β_{lim}, established by the standards [45]. Since the integrals needed to evaluate the reliability index are difficult to compute analytically, sampling techniques are usually employed for this purpose. Among these sampling techniques, Monte Carlo simulation will be adopted in this study [46].

Hence, the multi-objective function, $\{f(\{\theta\})\}$, of the motion-based design problem under the stochastic conditions may be re-formulated as the following reliability problem:

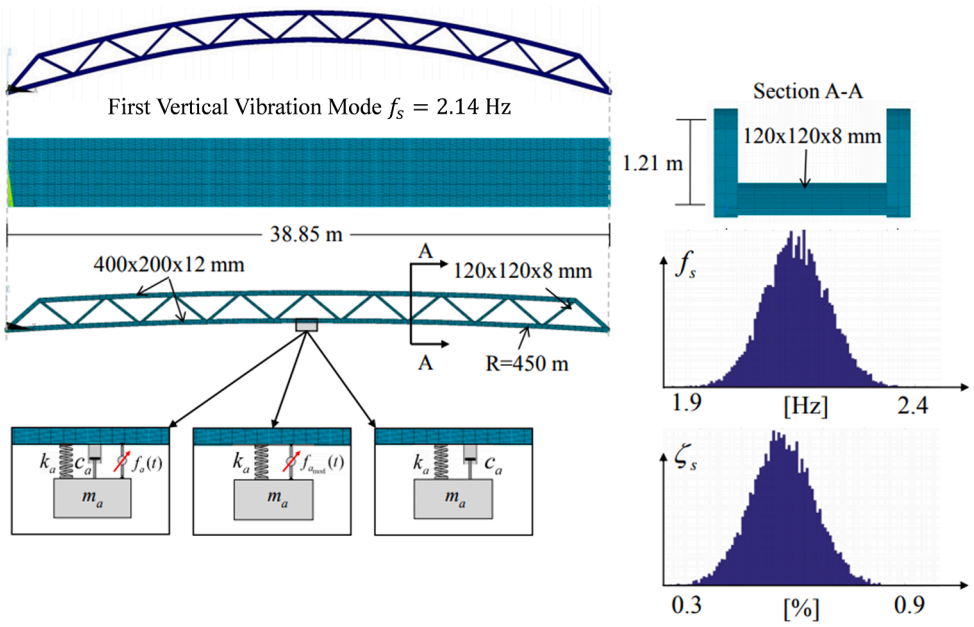

Fig. 6. Finite element model of the benchmark footbridge and first vertical vibration mode.

$$\{f(\{\theta\})\} = \{f_1(\{\theta\}) \quad f_2(\{\theta\})\} = \left\{\mu \quad \frac{\beta_{lim}}{\beta(\{\theta\})}\right\} \tag{30}$$

Accordingly, the additional condition for the solution of the subsequent decision-making problem may be re-formulated as $\frac{\beta_{lim}}{\beta(\{\theta\})} = 1$.

Finally, in order to summarize this section, Fig. 5 shows the flowchart of the proposed motion-based design method for the design of different TMD techniques under deterministic and stochastic conditions. Both the non-dominated Pareto front and the additional condition considered to solve the decision-making problem are also illustrated in Fig. 5.

4. Application example

Subsequently, a numerical case-study is presented herein to illustrate the practical implementation of the motion-based design method for the robust design of the abovementioned TMD techniques (Fig. 1) when they are used to mitigate the pedestrian-induced vibrations in lively steel footbridges under uncertainty conditions.

4.1. Description and modelling of the benchmark footbridge

For our purposes, a numerical footbridge, which is used by Setra guidelines [35] to describe how to assess numerically the VSLS has been adopted here as benchmark. The footbridge is a simple supported structure with a single span of 38.85 m of length. The main structural system is configured by two lateral Warren steel trusses. The trusses are curved with a vertical curvature radius of 450 m. The height of the trusses is 1.21 m and their lateral separation is 2.90 m. Both the upper and lower chords of the trusses consist of rectangular hollow section 400x200x12 mm, and the diagonal and strut elements consist of rectangular hollow section 120x120x8 mm. These trusses are braced transversally between their lower chords by strut elements. A deck of the footbridge is formed by a reinforced concrete slab of 0.10 m of thickness which rests on the strut elements configuring a composite steel–concrete section. The width of the concrete slab is 2.50 m. Fig. 6 shows the general configuration of this footbridge.

The finite element model of the footbridge was creating using the package Ansys [47]. Both beam elements, BEAM188 (2 nodes per element, 6 d.o.f. in each node), and shell elements, SHELL181 (4 nodes per element, 6 d.o.f. in each node) has been considered for this purpose. The finite element model of the footbridge is composed by a mesh of 646 beam elements and 540 shell elements (Fig. 6). A linear behavior is assumed for the constitutive law of both construction materials [48], reinforced concrete and steel. The mechanical properties adopted are: (i) for the reinforced concrete, a Young's modulus, $E_c = 31000$ MPa, a Poisson's ratio, $\upsilon_c = 0.20$ and a density, $\rho_c = 2500$ kg/m^3; and (ii) for the steel, a Young's modulus, $E_s = 210000$ MPa, a Poisson's ratio, $\upsilon_s = 0.30$ and a density, $\rho_s = 7850$ kg/m^3. The structural damping ratio of the structure, ζ_s, is assumed as 0.6 %, according to the recommendations of Synpex guidelines [4].

The numerical modal parameters of the footbridge have been obtained via a numerical modal analysis of the model. The natural frequency ($f_s = 2.14$ Hz) of the first vertical vibration mode (Fig. 6) and its associated modal mass ($m_s = 34706$ kg) have been determined. The natural frequency of this vibration mode is within the range (1.25 −2.30 Hz), that characterizes the pedestrian-structure interaction in vertical direction [4], so that it is expected that the footbridge may suffer from excessive vibrations and accordingly the VSLS may not be met (according to Synpex guidelines [4], the VSLS is met if the maximum vertical acceleration of the footbridge, $\ddot{x}_{s,max}(\{\theta\})$, is lower than an allowable acceleration, $\ddot{x}_{lim}$). In order to overcome this limitations, different TMD techniques will be designed considering the motion-based design method.

A typical design scenario for an urban footbridge has been taken into account herein. Thus, a walking pedestrian density (pedestrian traffic) of 1 P/m^2 (Table 1); and an allowable vertical acceleration, $\ddot{x}_{lim}$, of 1 m/s^2 (Table 2) have been considered.

Subsequently, the uncertainty of the modal properties of the structure has been taken into account in this study. For this purpose, both the first vertical natural frequency, f_s, and its associated damping ratio, ζ_s, are assumed as random variables which follow normal probabilistic distributions. According to the results of some recent studies [10,27], a variation range of ±10% and ±50% have been assumed respectively to characterize these functions (Fig. 6). Additionally, an allowable reliability index, β_{lim}, of 1.35 has been considered herein according to the recommendations of European standards [45].

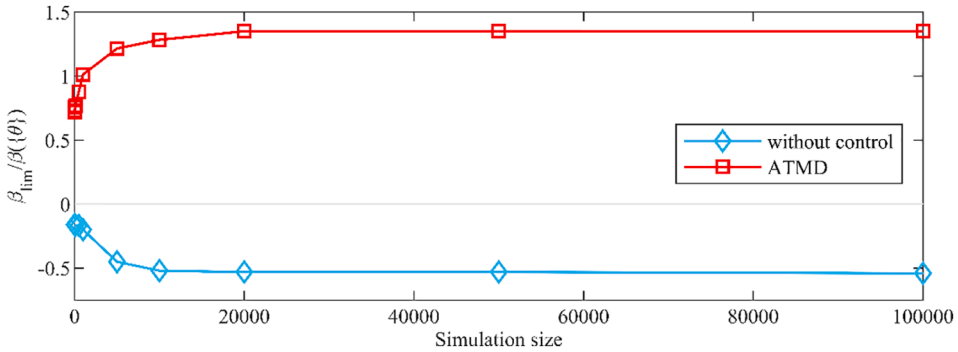

Fig. 7. Convergence analysis of the ratio, $\frac{\beta_{lim}}{\beta(\{\theta\})}$, in terms of the sampling size of the Monte Carlo simulation considering an allowable acceleration, $\ddot{x}_{lim} = 1$ m/s^2 and reliability index, $\beta_{lim} = 1.35$: (i) without ATMD (red line); and (ii) with an ATMD (blue line). (For interpretation of the references to colour in this figure legend, the reader is referred to the web version of this article.)

4.2. Motion-based design of the different TMD techniques under uncertainty conditions.

The motion-based design method, presented by Eqs. (24) and (30), is now applied for the robust design of three different TMD techniques (ATMD, STMD and PTMD). The formulation of the design problem for the three vibration absorbers shares the same multi-objective function but it differs both in the design variables and the search domain. A hybrid strategy has been considered for the intelligent control systems (ATMD and STMD). Thus, this design problem may be formulated as follows:

$$\begin{gathered}\text{Find } \{\theta\} \\ \text{Minimizing } \{f(\{\theta\})\} = \{f_1(\{\theta\}) \quad f_2(\{\theta\})\} = \left\{\mu \quad \frac{\beta_{lim}}{\beta\{\theta\}}\right\} \\ \text{Subjected to} \{\theta^l\} \le \{\theta\} \le \{\theta^u\}\end{gathered} \tag{31}$$

where the following design variables and search domain have been considered:

(i) for the ATMD, $\{\theta\} = \{\mu \quad \alpha_d \quad \beta_d\}$ $\left\{\theta^l\right\} = \{0.01 \quad 10 \quad 10^{-8}\}$ and $\{\theta^u\} = \{0.1 \quad 1000 \quad 10^{-5}\}$;

(ii) for the STMD, $\{\theta\} = \{\mu \quad \alpha_d \quad \beta_d\}$, $\left\{\theta^l\right\} = \{0.01 \quad 10 \quad 10^{-8}\}$ and $\{\theta^u\} = \{0.1 \quad 1000 \quad 10^{-5}\}$; and

(iii) for the PTMD, $\{\theta\} = \{\mu\}$, $\left\{\theta^l\right\} = \{0.01\}$ and $\{\theta^u\} = \{0.1\}$.

Additionally, for the STMD, the value of the driving force has been limited, ($f_{min} = 667$ N and $f_{max} = 2447$ N), according to the values recommended by a manufacturer [49].

In this manner, the main objective of this design problem is to find the robust optimum mechanical parameters of the three mentioned TMD techniques that minimizing the TMD mass guarantees the fulfilment of the design requirements (an allowable vertical acceleration, $\ddot{x}_{lim}$, of 1 m/s^2 considering a reliability index, β_{lim}, of 1.35).

The equations of motion of the TMD-footbridge interaction model have been integrated considering a step time of 0.01 sec and total duration of 10 sec. As global optimization algorithm, genetic algorithms have been employed to solve these minimization problems [25]. A Monte Carlo simulation was considered [46] to compute numerically the

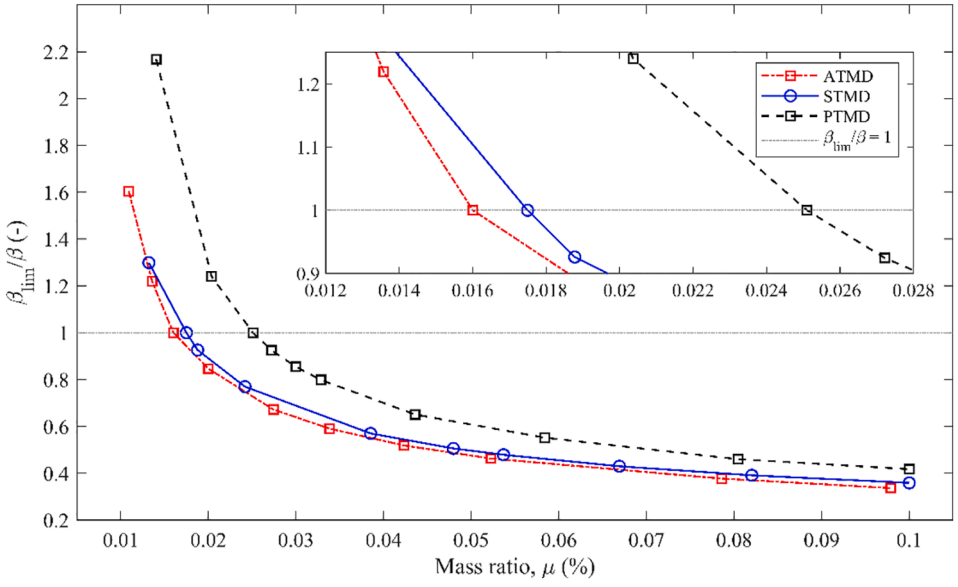

Fig. 8. Pareto front for the three different TMD techniques considered: (i) active (ATMD); (ii) semi-active (STMD); and (iii) passive (PTMD).

Table 3
Reliability index, $\beta(\{\theta\})$, of the VSLS of the footbridge (uncontrolled and controlled) and constituent parameters for the different TMD techniques designed according to the motion-based design method.

TMD	$\ddot{x}_{s,max}$[m/s^2]	$\beta(\{\theta\})$[–]	μ[%]	α_d[–]	β_d[–]	m_a[kg]	c_a[sN/m]	k_a[N/m]	$\lvert f_{,a}\rvert$[N]
No	11.42	−0.53	—	—	—	—	—	—	—
ATMD	1.00	1.35	1.61	357	$4.58{\cdot}10^{-6}$	555	1130	$9.73{\cdot}10^{4}$	685
STMD	1.00	1.35	1.75	481	$6.84{\cdot}10^{-6}$	607	—	$1.06{\cdot}10^{5}$	2447
PTMD	1.00	1.35	2.51	—	—	871	2189	$1.49{\cdot}10^{5}$	—

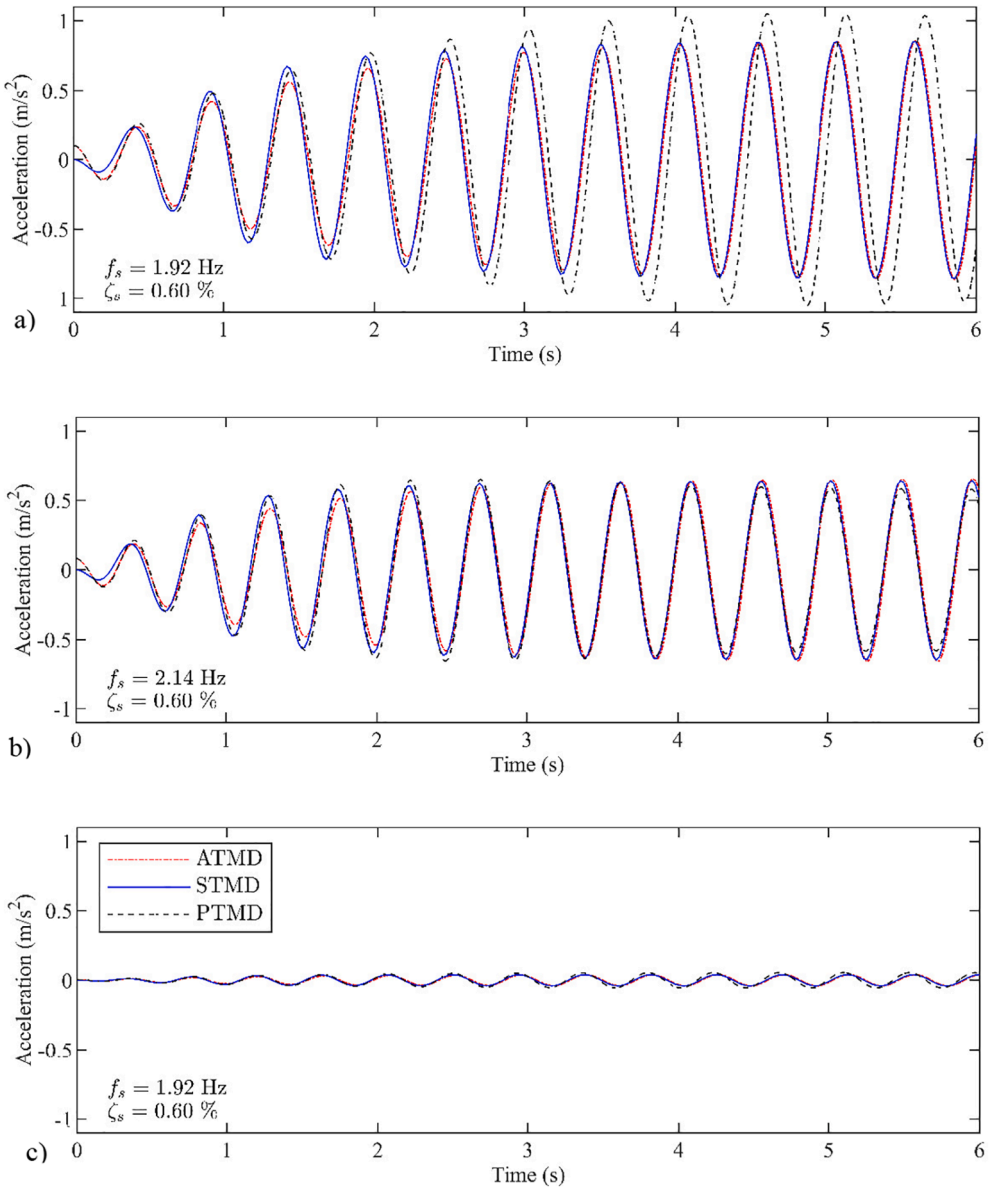

Fig. 9. Dynamic response (accelerations, $\ddot{x}_s(t)$) of the controlled footbridge considering the three different TMD techniques in terms of the variation of the natural frequency of the first vertical vibration mode of the footbridge: a) $f_s = 1.92$ Hz; b) $f_s = 2.14$ Hz; and c) $f_s = 2.29$ Hz. Damping ratio $\zeta_s = 0.6\%$ for the three illustrated cases.

reliability index, $\beta(\{\theta\})$. A convergence analysis was performed previously to determine the size of the Monte Carlo simulation. The evolution of this index, $\beta(\{\theta\})$, without and with ATMD, in terms of the sampling size has been analysed. Fig. 7 illustrates the result of this convergence analysis. As result of this convergence analysis, the sample size was set at 40,000 simulations (significance level of 0.01 and an accuracy of 0.01).

A flowchart of design process has been shown in Fig. 5. Additionally some illustrations explaining the different steps of the design process have been included in Fig. 5.

Fig. 8 shows the mentioned Pareto front, which illustrates the non-dominated best solutions of the optimization process for the three designed TMD techniques. The dependence between the reliability index, $\beta(\{\theta\})$, and the mass ratio, μ, is shown in Fig. 8. Finally, the additional condition, $\frac{\beta_{lim}}{\beta(\{\theta\})} = 1$, to solve the decision-making problem

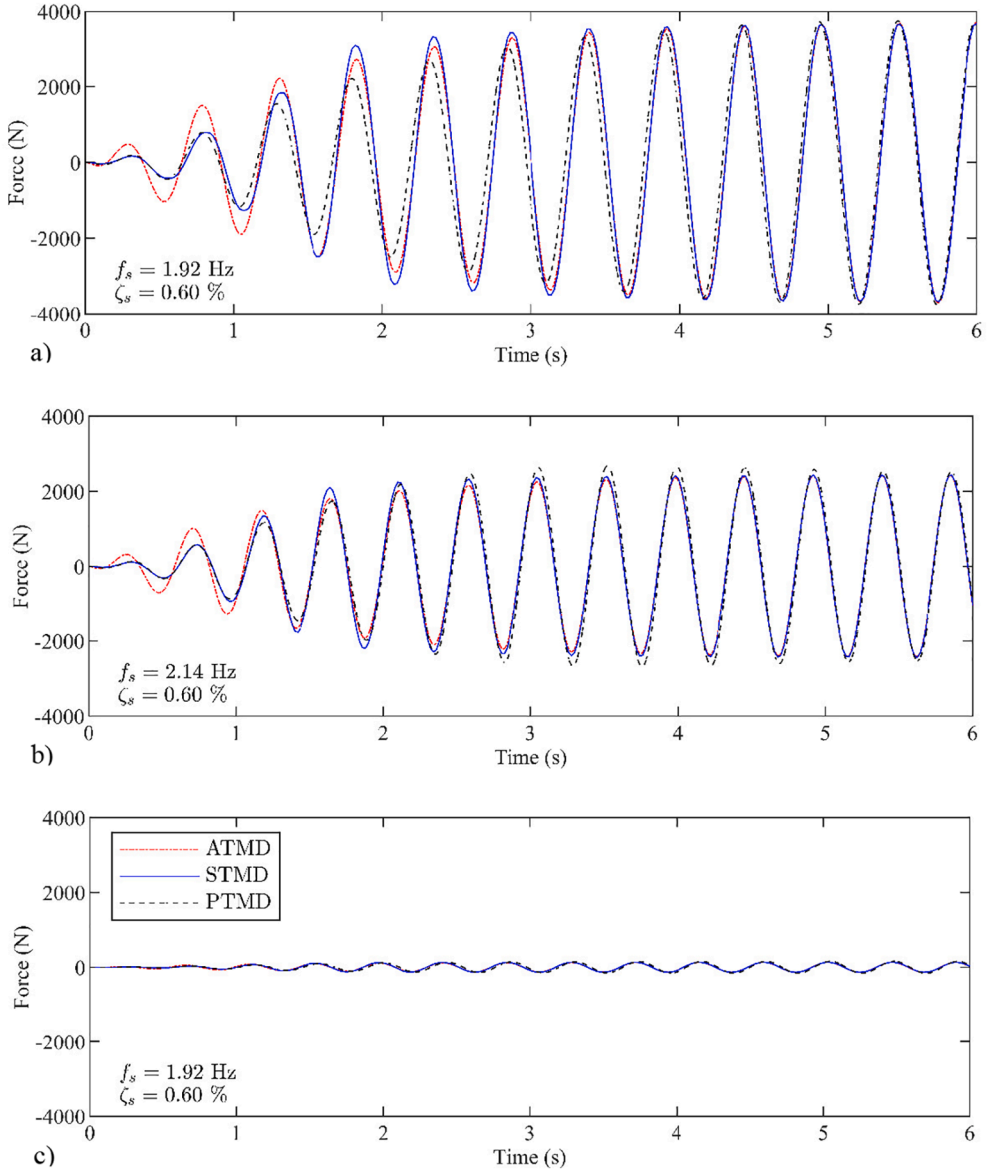

Fig. 10. Stiffness force of the three different TMD techniques in terms of the variation of the natural frequency of the first vertical vibration mode: a) $f_s = 1.92$ Hz; b) $f_s = 2.14$ Hz; and c) $f_s = 2.29$ Hz. Damping ratio $\zeta_s = 0.6\%$ for the three illustrated cases.

has been included for the sake of completeness.

As result of these design problems, Table 3 shows the reliability index, $\beta(\{\theta\})$, associated with the compliance of the VSLS of the footbridge without and with the three different TMD techniques. As Table 3 shows, the reliability index of the uncontrolled footbridge does not meet the VSLS then the different TMDs have been designed to achieve the fulfilment of the required limits. Thus, the different TMDs, designed according to the motion-based design method, allow controlling the dynamic response of the footbridge under uncertainty conditions without compromising their cost (the value of the reliability index for each case is equals to its allowable value). Finally, the parameters of the different TMDs (where $|f_a|$ is the maximum absolute value of the driving force) are included in Table 3. It is also shown in Table 3 the existing relation between the required TMD mass and the control technique considered to mitigate the pedestrian-induced vibrations in this footbridge. Furthermore, it is illustrated that the use of intelligent control systems (ATMD and STMD) allows achieving a considerable reduction of the TMD mass in exchange of employing an additional mechanical device (actuator or semi-active dashpot) powered by an external supply. Finally, the results, illustrated in Table 3, highlight both the ability of the different TMD techniques to control this vibration problem and the goodness of the proposal to establish a common framework for the design of the different TMD techniques when they are used to control the pedestrians-induced vibrations in slender footbridges under uncertainty conditions.

4.3. Discussion of the results

The dynamic behavior of the controlled footbridge using the three TMD techniques is now analyzed under the pedestrian stream defined by Eqn. (15). For this purpose, both the variation of the dynamic response (accelerations, $\ddot{x}_s(t)$) of the controlled footbridge and the interaction forces between each TMD technique and the footbridge in terms of the natural frequency of its first vertical vibration mode have been shown in Figs. 9–12.

Therefore, Fig. 9 shows the variation of the dynamic response; Fig. 10 shows the variation of the stiffness force, $k_a(x_a(t) - x_s(t)$; Fig. 11 shows the variation of the damping force plus the driving force (when it corresponds): (i) $c_a(x_a(t) - x_s(t) + f_a$ for the ATMD; (ii) $c_a(x_a(t) - x_s(t) + f_{a_{mod}}$ for the STMD; and $c_a(x_a(t) - x_s(t))$ for the PTMD);

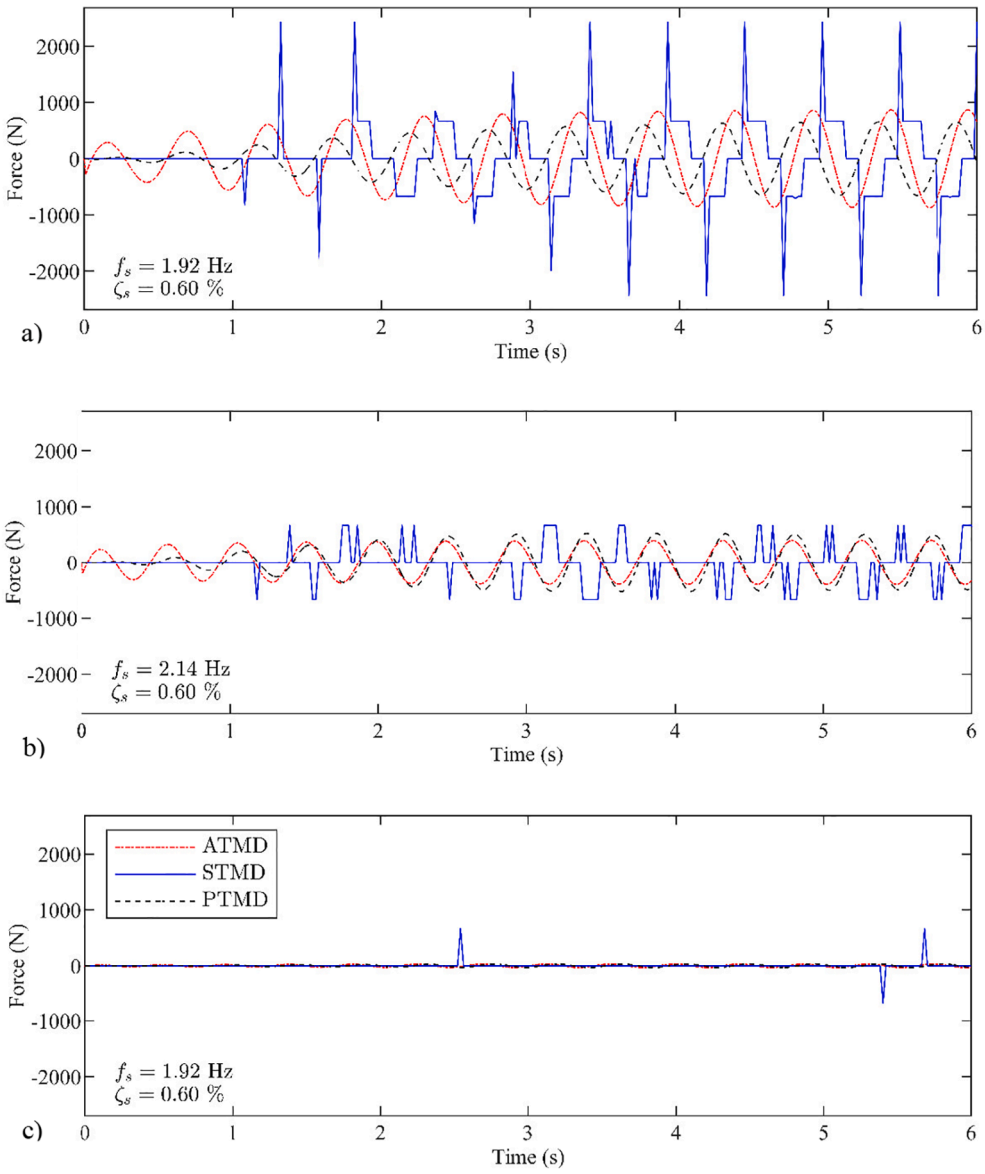

Fig. 11. Damping force plus the driving force (when it corresponds), of the three different TMD techniques in terms of the variation of the natural frequency of the first vertical vibration mode: a) $f_s = 1.92$ Hz; b) $f_s = 2.14$ Hz; and c) $f_s = 2.29$ Hz. Damping ratio $\zeta_s = 0.6\%$ for the three illustrated cases.

and Fig. 12 shows the variation of the overall control force.

Three representative cases have been shown: (i) a lower value of 1.92 Hz,; (ii) an average value of 2.14 Hz; and (iii) a upper value of 2.29 Hz (according to Synpex guidelines [4] if the considered natural frequency is greater than 2.3 Hz the value of the vertical walking pedestrian load is equals to zero due to the value of factor, $\psi(f_p)$, computed by Eqn. (17)). It is assumed an average damping ratio, ζ_s, of 0.6 % for all the considered cases.

As, Fig. 9 illustrates the structural uncertainties cause the detuning of the TMD. Fig. 9a shows that this detuning phenomenon is reflected in the design of the different TMD techniques. ATMD and STMD present a better behavior under uncertainty conditions (a better attenuation of the dynamic response with a lower mass ratio). Additionally, Fig. 9a shows a different phase among the dynamic response of the controlled footbridge among the three different TMD techniques. Fig. 9b shows that the dynamic response of the controlled footbridge under resonance conditions is similar for the three considered techniques.

Fig. 10 illustrates that the stiffness force has a similar behavior than the abovementioned dynamic response. In relation to the damping force plus the driving force, Fig. 11 illustrates as the effect of these forces is remarkable when the structural uncertainties cause the detuning of the vibration absorber. As it is shown in Fig. 11a in these circumstances, the component associated with the driving force is highlighted. A different phase is also shown in Fig. 11 for the damping force plus the driving force for the three different TMD techniques. Additionally, Fig. 12 shows that the stiffness force has the greatest weight in the overall control force for the different TMD techniques. Furthermore, a remarkable effect is shown in both Fig. 11 and Fig. 12, the spikes in the damping force of the STMD. As it has been mentioned previously, the semi-active dashpot has been simulated via a clipped driving force (obtained by the LQR algorithm). As the real semi-active dashpot cannot operate in the four quadrats of the force–velocity space, but only in the two purely dissipative quadrats [50], there are temporal instants in which the semi-active control comes into operation producing these characteristic spikes. This effect has been recently reported in literature by other researchers [51].

Finally, in view of all these results, it can also be concluded that the proposed method allows establishing a common framework which assists engineering practitioners in the robust design of different TMD techniques when these vibration absorbers are used to mitigate the

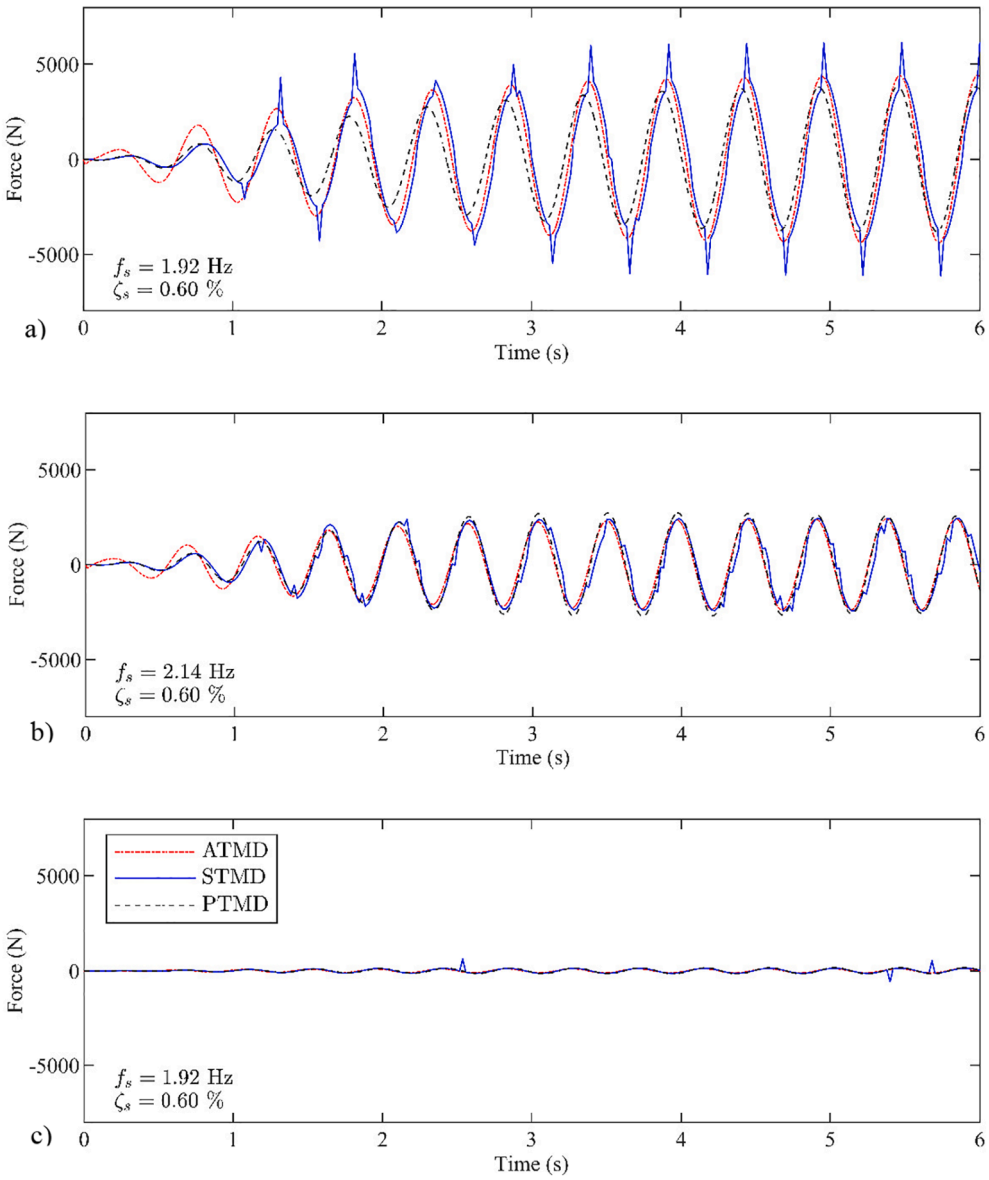

Fig. 12. Overall control force of the three different TMD techniques in terms of the variation of the natural frequency of the first vertical vibration mode: a) $f_s = 1.92$ Hz; b) $f_s = 2.14$ Hz; and c) $f_s = 2.29$ Hz. Damping ratio $\zeta_s = 0.6\%$ for the three illustrated cases.

pedestrian-induced vibrations in slender footbridges under uncertainty conditions. Thus, the proposed method can be used as a computational tool to easily implement different TMD techniques during the design phase of slender footbridges equipped with these vibration absorbers. Accordingly, the proposed method makes easier the design of integrated TMD-footbridges system which can enhance the search of new forms and structural systems without compromising the fulfilment of the VSLS of the structure.

5. Conclusions

In this manuscript, a common framework for the robust design of different TMD techniques (active, semi-active and passive), when these vibrations absorbers are used to mitigate the pedestrian-induced vibrations in lively footbridges, is proposed. The framework is based on the implementation of the motion-based design method under uncertainty conditions. According to this method, the design problem may be transformed into the combination of two sub-problems: (i) a multi-objective optimization sub-problem; and (ii) a decision-making sub-problem.

The multi-objective optimization sub-problem may be formulated as follows:

(i) the design variables are both some mechanical parameters of the TMD and the driving force of the actuator (for ATMD and STMD cases);
(ii) the different elements of the multi-objective function are defined in terms of the cost of the vibration absorber and the fulfilment of the VSLS of the controlled structure;
(iii) a search domain is considered to ensure the physical meaning of the solutions obtained.
(iv) nature-inspired computational algorithm (genetic algorithms have been used herein) are usually considered to cope with this problem due to the non-linear relationship between the objective function and the design variables.

As result of this optimization problem, a set of non-dominated solutions, the so-called Pareto front, is obtained. Hence, an additional condition has been included herein to solve this decision-making problem, the selection of the best solution among the different elements of

the Pareto front.

As the main objective of any vibration absorber is to control the excessive vibrations of the main structure during its overall life cycle, the design requirements are normally defined in terms of the VSLS. Additionally, in order to guarantee the robustness of the design under the structure uncertainties and tuning errors, the VSLS is re-formulated according to a reliability analysis method. For this purpose, a reliability index, $\beta\{\theta\}$, which indicates the probability of compliance of this limit state, is considered herein. Sampling techniques, as the Monte Carlos simulation method, are usually used to determine numerically this index.

As application example, a numerical footbridge, which is prone to vibrate due to vertical walking pedestrian action, has been considered. Three different TMD techniques (active, semi-active and passive) have been installed at its mid-span to mitigate the pedestrian-induced vibrations. The mechanical parameters and the driving force (when it corresponds) of these vibration absorbers have been obtained via the implementation of this proposal. As result of this study, the performance of the proposed method has been shown up and the possibility to design different TMD techniques using a common framework has been highlighted.

In spite of its good performance, further studies are needed, both to better determine the probabilistic distribution function of the modal properties of the structure and to assess experimentally the performance of the structure controlled by smart tuned mass dampers designed according to this proposal.

Declaration of Competing Interest

The authors declare that they have no known competing financial interests or personal relationships that could have appeared to influence the work reported in this paper.

Acknowledgements

This work was partially funded by two research projects: (i) RTI2018-094945-B-C21 (Ministerio de Economía y Competitividad of Spain and the European Regional Development Fund); and (ii) SEED-SD RTI2018-099639-B-I00 (Ministerio de Ciencia, Innovación y Universidades of Spain).

References

[1] Van Nimmen K, Lombaert G, De Roeck G, Van den Broeck P. Vibration serviceability of footbridges: evaluation of the current codes of practice. Eng Struct 2014;59:448–61.
[2] Ahmadi E, Caprani C, Živanović S, Heidarpour A. Experimental validation of moving spring-mass-damper model for human-structure interaction in the presence of vertical vibration. Structure 2020;29:1274–85.
[3] Weber F, Feltrin G and Hult O (2006). Guidelines for structural control. Dubendorf, Switzerland: Structural Engineering Research Laboratory, Swiss Federal Laboratories for Materials Testing and Research.
[4] Butz CH, Heinemeyer CH, Goldack A, Keil A, Lukic M, Caetano E and Cunha A (2007). Advanced Load Models for Synchronous Pedestrian Excitation and Optimised Design Guidelines for Steel Footbridges (SYNPEX). RFCS-Research Project RFS-CR-03019.
[5] Connor J, Laflamme S. Structural motion engineering. Springer International Publishing; 2014. p. 626.
[6] Preumont A, Seto K. Active control of structures. 1st ed. Cornwall: John Wiley & Sons Ltd; 2008. p. 312.
[7] Casciati F, Magonette G, Marazzi F. Technology of semiactive devices and applications in vibration mitigation. 1st ed. Chichester: John Wiley & Sons Ltd.; 2006. p. 269.
[8] Elias S, Matsagar V. Research developments in vibration control of structures using passive tuned mass dampers. Annu Rev Control 2017;44:129–56.
[9] Wang L, Nagarajaiah S, Shi W, Zhou Y. Semi-active control of walking-induced vibrations in bridges using adaptive tuned mass damper considering human-structure-interaction. Eng Struct 2021;244:112743.
[10] Hu W-H, Caetano E, Cunha A. Structural health monitoring of a stress-ribbon footbridge. Eng Struct 2012;57:578–93.
[11] Wamg L, Shi W, Ying Z, Zhang Q. Semi-active eddy current pendulum tuned mass damper with variable frequency and damping. Smart Struct Syst 2020;25(1):65–80.
[12] Jiménez-Alonso JF, Naranjo-Pérez J, Díaz IM, Sáez A. Motion-based design of vibrating civil engineering structures under uncertainty conditions. Struct Concr 2020;21(6):2339–52.
[13] Shi W, Wang L, Lu Z. Study on self-adjustable tuned mass damper with variable mass. Struct Control Health Monit 2018;25(3):e2114.
[14] Li C, Liu Y. Hybrid active tuned mass dampers for structures under the ground acceleration. Earthq Eng Struct D 2015;31(5):1041–52.
[15] Moutinho C, Cunha A, Caetano E, de Carvalho JM. Vibration control of a slender footbridge using a passive and a semi-active tuned mass damper. Struct Contr Health Monit 2018:e2208.
[16] Rathi AK, Chakraborty A. Reliability-based performance optimization of TMD for vibration control of structures with uncertainty in parameters and excitation. Struct Control Health Monit 2016:e1857.
[17] Kaveh A, Javadi SM, Mahdipour MR. Optimal structural control of tall buildings using tuned mass dampers via chaotic optimization algorithm. Str 2020;28:2704–13.
[18] De Domenico D, Ricciardia G, Takewaki I. Design strategies of viscous dampers for seismic protection of building structures: a review. Soil Dyn Earthq Eng 2019;118:144–65.
[19] Asami T, Nishihara O, Baz AM. Analytical solutions to H_∞ and H_2 optimization of dynamic vibration absorbers attached to damped linear systems. J Vib Acoust 2002;124(2):284–95.
[20] Lagaros ND, Plevris V, Mitropoulou CC. Design optimization of active and passive structural control systems. IGI Global Publisher; 2013. p. 444.
[21] Liang QQ. Performance-based optimization: a review. Adv Struct Eng 2007;10:739–53.
[22] Ferreira F, Moutinho C, Cunha Á, Caetano E. Proposal of optimum tuning of semiactive TMDs used to reduce harmonic vibrations based on phase control strategy. Struct Control Health Monit 2018:e2131.
[23] Xu ZD, Guo YQ, Zhu JT, Xu FH. Intelligent vibration control in civil engineering structures. 1st ed. London: Academic Press-Elsevier; 2017. p. 264.
[24] Wang X, Pereira E, García-Palacios JH, Díaz IM. A general vibration control methodology for human-induced vibrations. Struct Control Health Monit 2019.
[25] Mohebbi M, Shakeri K, Ghanbarpour Y, Majzoub H. Designing optimal multiple tuned mass dampers using genetic algorithms (GAs) for mitigating the seismic response of structures. J Vib Control 2013;19(4):605–25.
[26] Zivanović S and Pavic A. Probabilistic Assessment of Human Response to Footbridge Vibration. J Low Freq Noise V A. 2009; 28(4): 255–268.
[27] Soria JM, Díaz I, García-Palacios J, Ibán N. Vibration monitoring of a steel-plated stress-ribbon footbridge: uncertainties in the modal estimation. J Bridge Eng 2016;21:C5015002.
[28] Shi W, Wang L, Lu Z, Wang H. Experimental and numerical study on adaptive-passive variable mass tuned mass damper. J Sound Vib 2019;452:97–111.
[29] Wang L, Shi W, Zhang Q, Ying Z. Study on adaptive-passive multiple tuned mass damper with variable mass for a large-span floor structure. Eng Struct 2020;209:110010.
[30] Jimenez-Alonso JF, Saez A. Motion-based design of TMD for vibrating footbridges under uncertainty conditions. Smart Struct Syst 2018;21(6):727–40.
[31] Souza de Cursi E, Sampaio R. Uncertainty quantification and stochastics modeling with matlab. 1st ed. London: ISTE Press Ltd; 2015. p. 442.
[32] Lievens K, Lombaert G, De Roeck G, Van den Broeck P. Robust design of a TMD for the vibration serviceability of a footbridge. Eng Struct 2016;123:408–18.
[33] Holický M. Reliability analysis for structural design. 1st ed. Stellenbosch: Sun Press; 2009. p. 199.
[34] Aggumus H, Cetin S. Experimental investigation of semiactive robust control for structures with magnetorheological dampers. J Low Freq Noise V A 2018;37(2):216–34.
[35] Setra/AFGC Guide méthodologique passerelles piétonnes (Technical Guide Footbridges: Assessment of vibration behaviour of footbridge under pedestrian loading); 2006.
[36] Moutinho C. Testing a simple control law to reduce broadband frequency harmonic vibrations using semi-active tuned mass dampers. Smart Mater Struct 2015;24:055007.
[37] Weber C. Semi-active vibration absorber based on real-time controlled MR damper. Mech Syst Signal Process 2014;46:272–88.
[38] Ferreira F, Moutinho C, Cunha A, Caetano E. Use of semi-active tuned mass dampers to control footbridges subjected to synchronous lateral excitation. J Sound Vib 2019;446:176–94.
[39] Den Hartog JP. Mechanical vibrations. New York: McGraw-Hill; 1947. p. 464.
[40] Magdaleno A, Pereira E, Reynolds P, Lorenzana A. A common framework for tuned and active mass dampers: application to a two-storey building model. Exp Tech 2021 (on line).
[41] Xu ZD, Sha LF, Zhang XC, Ye HH. Design, performance test and analysis on MR damper for earthquake mitigation. Struct Control Health Monit 2012;20(6):956–70.
[42] Zhang XC, Xu ZD. Testing and modeling of a CLEMR damper and its application in structural vibration reduction. Nonlinear Dyn 2012;70(2):1575–88.
[43] Matlab R2020a. http://www.mathworks.com/.
[44] ISO 2394 (2015). General principles on reliability for structures.
[45] Eurocode 0 (2002). EN 1990. Basis of structural design. European Committee for Standardization.
[46] Binder K, Heermann D. Monte Carlo Simulation in Statistical Physics. An Introduction. 1st ed. Berlin. Springer-Verlagr; 2010, p.202.
[47] Ansys (2020) Mechanical Release http://www.ansys.com/.
[48] Eurocode 3 (2005). EN 1993-1-1: Design of steel structures - Part 1-1: General rules and rules for buildings. European Committee for Standardization.

[49] LORD (2020) RD-8040-1 damper https://www.lord.com/.
[50] Soria JM, Díaz IM, García-Palacios JH. Further steps towards the tuning of inertial controllers for broadband-frequency-varying structures. Struct Control Health Monit 2020;27(1):e2461.
[51] Moutinho C. Testing a simple control law to reduce broadband frequency harmonic vibrations using semi-active tuned mass dampers. Smart Mater Struct 2015;24(5):055007.